Geophysical Research Letters

RESEARCH LETTER
10.1029/2020GL089001

Special Section:
Fire in the Earth System

Extreme Pyroconvective Updrafts During a Megafire

B. Rodriguez[1,2], N. P. Lareau[3], D. E. Kingsmill[4], and C. B. Clements[1]

[1]Department of Meteorology and Climate Science, San José State University, San José, CA, USA, [2]National Weather Service, San Diego, CA, USA, [3]Department of Physics, University of Nevada, Reno, Reno, NV, USA, [4]Cooperative Institute for Research in Environmental Sciences, University of Colorado Boulder, Boulder, CO, USA

Abstract Airborne cloud radar reveals extreme wildfire updrafts (~60 m s^{-1}) and downdrafts (~30 m s^{-1}) rivaling those in supercell thunderstorms. These extreme vertical velocities occur through a 3-km-deep layer and below the base of a developing pyrocumulonimbus (pyroCb) cloud, which extends to the tropopause at 12 km. In situ aircraft sampling shows updrafts are linked to large temperature and moisture excesses but remain subsaturated at flight level (i.e., below cloud base). Parcel estimates using the in situ data help explain how these "hot-moist" updrafts trigger the overlying pyroCb. The extreme vertical motions observed also pose a previously undocumented aviation hazard.

Plain Language Summary Massive wildfires (i.e., megafires) produce enough heat to generate powerful updrafts that are as strong as those observed during tornadic supercell thunderstorms. Weather radar data show that these updrafts are as strong as 130 mph (209 km/hr) and extend for miles above the surface. These updrafts can trigger fire-generated thunderstorms and pose a threat to aircraft flying in the vicinity of large wildfires.

Key Points:
- Megafires produce extreme updrafts rivaling those in supercell thunderstorms.
- These updrafts help trigger pyrocumulonimbus clouds that reach to the tropopause

Supporting Information:
- Supporting Information S1
- Figure S1
- Figure S2
- Table S1
- Table S2
- Table S3

Correspondence to:
B. Rodriguez,
bruno.rodriguez@noaa.gov

Citation:
Rodriguez, B., Lareau, N. P., Kingsmill, D. E., & Clements, C. B. (2020). Extreme pyroconvective updrafts during a megafire. *Geophysical Research Letters*, *47*, e2020GL089001. https://doi.org/10.1029/2020GL089001

Received 23 MAY 2020
Accepted 2 SEP 2020
Accepted article online 9 SEP 2020

1. Introduction

Wildfire convective plumes contribute to extreme fire behavior (Werth et al., 2011), yet their internal structure and dynamics remain seldom observed and poorly understood, especially during large and destructive wildfires. As a result, simple questions such as "how strong are wildfire updrafts?" remain largely unanswered, presenting a critical gap in our understanding given that updrafts necessitate vigorous inflows that impact fire spread and firefighter safety (Peace et al., 2017), loft embers large distances ahead of a fire front (Thurston et al., 2017), initiate fire-generated thunderstorms (i.e., pyrocumulonimbus, hereafter "pyroCb"; Fromm et al., 2010; Lareau & Clements, 2016; Peterson et al., 2017), and even contribute to deadly fire-generated vortices (Cunningham & Reeder, 2009; Fromm et al., 2006; Lareau et al., 2018). Confronting this knowledge gap, we present first-of-their-kind airborne radar and in situ (flight level) observations that elucidate the velocity and thermodynamic structure of a deep pyroconvective plume generated by the Pioneer "megafire," which occurred in Idaho during the summer of 2016. As we will show, the vertical velocities in the observed plumes are extreme, rivaling those in tornadic and supercell thunderstorms.

2. Data and Methods

2.1. UWKA

Data in this study were primarily collected with the University of Wyoming King Air (UWKA), which was flown above the active perimeters of the Pioneer Fire to quantify the plume dynamics. The UWKA is equipped with a suite of in situ and remote sensing instrumentation (Wang et al., 2012), including the following:

2.1.1. WCR

Vertical velocity and radar reflectivity observations were obtained from the 93 GHz (3-mm wavelength) Wyoming Cloud Radar (WCR), which has a sensitivity of −25–40 dbZ, an accuracy of ~3 dbZ, a Nyquist velocity of ±15.8 m s^{-1}, and uses a range-gate resolution of 15 m. The data in this study are from the WCR's down-nadir antenna, which looks down into the wildfire plume from above (Damiani & Haimov, 2006). The WCR is sensitive to backscatter from pyrometeors (e.g., ash, Banta et al., 1992; McCarthy et al., 2019), such that the Doppler radial velocity provides a measure of in-plume vertical air motion and the reflectivity is proportional to the number and size of the scatterers. In order to address radial velocity aliasing in the WCR data, a continuity-based dealising technique (Bargen & Brown, 1980; Eilts & Smith, 1990; Ray &

Ziegler, 1977) was applied. Details of the radar post processing, including examples of the unfolding of aliased radial velocity data, are contained in the supporting information (Text S1).

2.1.2. In Situ Sensors

Aircraft in situ data are used to describe the in-plume and ambient thermodynamics at flight level. The details of the in situ sensors are summarized in Table S1. These sensors provide observations of (1) the potential temperature, (2) the horizontal (east-west and north-south) and vertical winds at aircraft level, and (3) the flight level relative humidity and water vapor mixing ratio. Aircraft altitude and GPS-derived latitude and longitude were also recorded.

2.2. Ancillary Data

Ancillary data used to contextualize the UWKA observations include the following:

1. Data from the National Weather Service (NWS) radar in Boise, Idaho (KCBX), located ~75 miles (120 km) from the northern perimeter of the fire, are used to characterize macroscopic details of the plume evolution. The specific data streams used are the "echo tops" product, which are the maximum height at which reflectivity >18 dbZ are detected and the radar reflectivity. The KCBX metadata are listed in Table S2.
2. Data from a weather balloon launched at 00 UTC on 30 August 2016 are used to characterize the ambient temperature and moisture profiles upstream of the Pioneer Fire. The sounding site is located at the Boise International Airport (KBOI). Additional details of the radiosonde are available in Table S2 and a Skew-T diagram is provided in Figure S2.
3. Fire perimeters produced by the National Infrared Operations (NIROPS) are used to quantify daily changes in fire area and were obtained from the National Interagency Fire Center (NIFC) (https://ftp.nifc.gov/public/incident_specific_data/great_basin/2016_Incidents/Pioneer/).
4. Local weather data proximal to the fire (Table S3) are obtained from Mesowest (Horel et al., 2002).

3. Results

3.1. The Fire and the Plume

The Pioneer Fire consumed a total of 76,081 ha (188,000 acres, 761 km^2) from 18 July to 15 September 2016 in Idaho, USA (Figure 1a), and reached 100% containment on 3 November 2016 after burning for 3.5 months. Although the term "megafire" lacks a common definition, it is most frequently ascribed size-based definitions (Buckland, 2019). For the purpose of this article, we adopt the definition used by the NIFC, which uses a minimum size of 100,000 acres (40,469 ha) as the criteria (Lindley et al., 2019). The focus of this paper is on a deep pyroCb-topped plume associated with a rapid 11,736 ha (29,000 acres) northeastward advance of the fire on 29 August 2016 (compare black and red perimeters in Figure 1a). The KCBX radar echo tops (Figure 1a) indicate that the plume extended from the surface (~2 km) to 12 km aloft (all heights are above sea level) with the deepest portion of the plume displaced northeast of the fire by the prevailing southwest winds. The plume height time series (Figure 1b) shows that the plume nearly doubled in vertical extent during the pyroCb initiation, which occurred starting at ~2300 UTC. The estimated plume top temperature at ~12 km was −55°C, based on radiosonde and satellite data (not shown), confirming the presence of glaciated clouds and therefore pyroCb classification (Peterson et al., 2017). There was no observational evidence that the plume produced precipitation.

Plume updrafts and downdrafts were sampled with the WCR mounted on the UWKA during the period of rapid plume growth (red shading Figure 1b). The aircraft flew three times above the advancing head fire plume (flight paths [Legs 9, 10, 13] and location indicated in Figures 1a and 1c) and once through a portion of the flanking fire plume (flight path [Leg 2] and location indicated in Figures 1a and 1c), at altitudes of ~7.7 and ~5.2 km respectively. Figure 1d shows the deep upright portion of this plume rising from the "head fire," along with the transition from an ash-filled lower plume to a pyroCb aloft. The flight paths pertaining to Legs 9, 10, and 13 were associated with laminar and stable flow conditions above the primary head fire plume, and as such were not subject to turbulence of any significance. Although uncertainty in the mean Doppler velocity may be increased during the turbulent penetration (Leg 2), no systematic bias would be incurred (S. Haimov, personal communication, June 16, 2020).

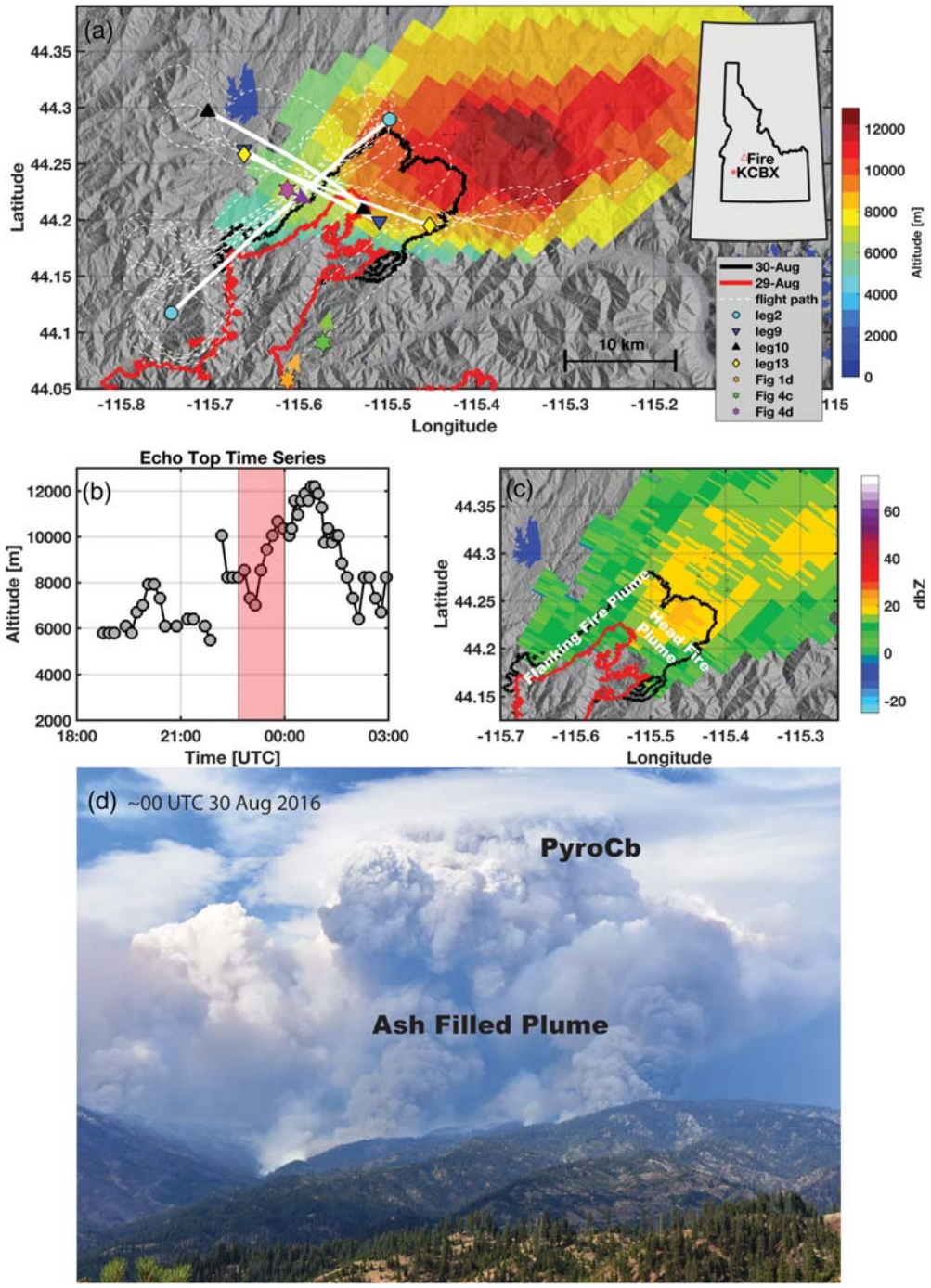

Figure 1. Overview of the PyroCb topped plume rising from the Pioneer Fire on 29 August 2016. (a) Map showing the fire perimeters, flight legs, locations of photos (triangle markers), terrain (hillshaded), and KCBX radar-derived plume "echo top" heights (color shaded). (b) KCBX echo top time series showing rapid plume growth and the flight interval (red shaded). (c) Time mean KCBX radar reflectivity during the flight interval with head and flanking fire plumes annotated. (d) Photograph from the Boise National Forest at ~00 UTC 30 August 2016 showing the head fire plume and the transition from the ash-filled lower plume to the pyroCb aloft.

3.2. Plume Vertical Velocity

The radar Doppler velocity observations reveal extreme updrafts and downdrafts in the developing head fire plume (Figures 2a–2c). The first radar overpass (Leg 9, Figure 2a) indicates two distinct convective elements: (1) a starting plume (Turner, 1962) extending from the surface to ~4.7 km and (2) a detached convective

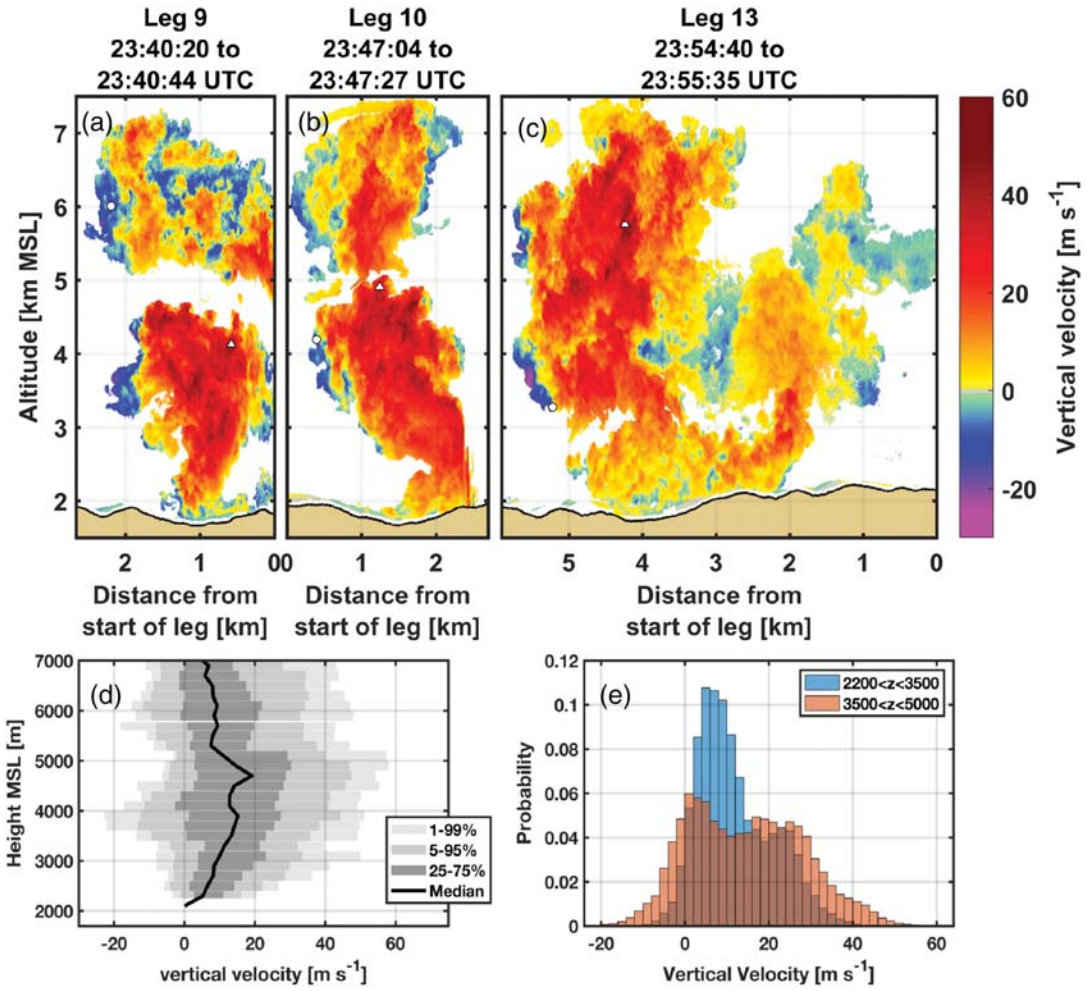

Figure 2. Vertical velocity observations and statistics for the head fire plume. (a–c) Radar Doppler velocity observations of the plume structure during Legs 9, 10, and 13. Warm (cool) colors represent updrafts (downdrafts). (d) Percentile ranges of vertical velocity as a function of height. (e) Probability density functions of vertical velocity for the lower and middle portions of the plume.

element aloft (5–7.25 km). The starting plume expands laterally with height (~2 km at its widest), culminating in a "cap," and exhibits strong central updrafts (max 40.1 m s^{-1}, triangle marker Figure 2a) flanked by narrow downdrafts (up to 18 m s^{-1}) along the plume periphery, a manifestation of horizontal vortex rings known to form on plume edges (Cunningham et al., 2005; Forthofer & Goodrick, 2011; Haines & Smith, 1987). In contrast the detached convective element aloft, likely from a previous convective "pulse" and indicating the presence of a horizontal-axis vortex structure entraining ash-free ambient air directly below it, contains weaker updrafts and downdrafts relative to the plume below.

The second overpass (Leg 10) reveals plume growth and intensification (Figure 2b). The maximum vertical velocity in the plume increased to 58.3 m s^{-1} (130.4 mph; 209.9 km/hr) at ~4.8 km (triangle marker in Figure 2b), marking the highest velocity observed during the campaign. This extreme updraft occurred within a small (~500 m wide) turret along the plume "cap" and above a 2-km-wide region encompassing numerous additional updraft cores exceeding 50 m s^{-1}. Commensurate with the extreme updrafts, vigorous downdrafts reaching −29.3 m s^{-1} were present along the plume edges. Further aloft, the detached convective element also grew and intensified during this time.

During the third overpass (Leg 13, Figure 2c), the gap between the lower starting plume and the upper convective element was absent, likely due to the flight path displaced farther northeast (see Figure 1a). Strong updrafts persisted aloft, (48 m s^{-1}, triangle marker Figure 2c), while near-surface updrafts diminished.

This may be due to the slanting (southwest-to-northeast) nature of the convective plume, which places this portion of the plume farther downwind of the surface combustion relative to previous overpasses.

The variation of vertical velocity with height is summarized by aggregating statistics for the three overpasses of the head fire plume (Figures 2d and 2e). These data show that the median and upper percentiles of vertical velocity increase with height up to ~4.8 km (Figure 2d). This implies that the plume retains a positively buoyant parcel over this depth, yielding sustained acceleration. Likewise, the lower plume is characterized by larger kurtosis, whereas farther aloft the distribution becomes bimodal and broader, with both stronger updrafts and downdrafts (Figure 2e). This is consistent with the occurrence of accelerating parcels and compensating mechanically forced downdrafts, which are approximately half of the updraft magnitude. Farther aloft (above 4.8 km), the velocity decreases with height, suggesting most parcels become negatively buoyant and decelerate.

3.3. Plume and PyroCb Thermodynamics

The increase in vertical velocity with height shown in Figure 2d is hypothesized to be driven by the sustained positive buoyancy (i.e., temperature anomaly) of the updraft parcels. While in situ (i.e., flight level) sampling of the head fire plume was not possible due to safety concerns, we are able to test this hypothesis using the observed thermodynamics of a 35 m s^{-1} updraft sampled during the aircraft penetration of the flanking plume at an altitude of ~5.2 km (Figure 3). The pronounced updraft is apparent in both the radar Doppler velocity (Figure 3a) and in situ velocity (blue line, Figure 3b) at approximately 4 km into the flight track. The corresponding potential temperature data (red line, Figure 3b) reveal the updraft is ~4.6 K warmer than the mean temperature along the flight leg and that the temperature structure is well correlated with the vertical motion observed at flight level, lending further validity to the in situ UWKA data. These data clearly indicate that the updraft core remains positively buoyant far above the surface despite substantial adiabatic cooling and entrainment dilution. This is consistent with thermodynamic modeling suggesting ambient entrainment must be sufficiently high to allow for plume condensational processes to occur yet restricted enough for the plume core to retain positive buoyancy until its condensation level (Tory et al., 2018).

We further hypothesize that the observed updraft temperature excess is a result of fire sensible heat flux alone, as opposed to latent heat release due to condensation in the pyroCb. This is tested using the updraft relative humidity (~70%, Figure 3c) and liquid water content (not shown), which both indicate subsaturated conditions and confirm that the aircraft penetration occurred below pyroCb cloud base (the height of which we estimate below). Notably, despite the subsaturated conditions, the in-plume water vapor mixing ratios are much larger than the environment at that level. The in-plume values exceed 3 g kg^{-1}, with a maximum of 3.8 g kg^{-1} collocated with the strongest updraft (Figure 3c), whereas the ambient environment is much drier (~1 g kg^{-1}), evidenced by step-like changes between moist and dry air as the aircraft moved in and out of plume elements (gray shading, Figures 3b and 3c). We also note that the updraft water vapor content is consistent with surface observations, which have a mean of ~3.7 g kg^{-1} (Table S3), suggesting the plume acquires a mixing ratio near that of the environment by entrainment, though the combustion contribution to the water vapor is unknown (Cunningham & Reeder, 2009; Luderer et al., 2009; Potter, 2005). This underscores the ability of plume updraft cores to function as a pathway for the transfer of near-surface properties to the upper troposphere.

These hot, moist plume cores are important for initiating the overlying pyroCb, which subsequently releases moist instability and enables the plume to reach the tropopause. This can be seen by estimating the dry- and moist-parcel ascent above flight level relative to the ambient environment as characterized by aircraft and radiosonde profiles (Figures 4a and 4b). Using the median in-plume parcel properties (+1.0 K, 3.1 g kg^{-1}, black line Figure 4b), we find that the plume condenses at 5,945 m (green square, Figure 4b) and quickly becomes negatively buoyant in the overlying stratified layer. In contrast the hottest, wettest plume parcels (+4.6 K, 3.8 g kg^{-1}, green line Figure 4b) condense at 6,036 m (green diamond, Figure 4b) and remain weakly buoyant up to ~12 km where they encounter the tropopause (black dashed line). Based on these observations and parcel estimates, it is likely that the "hot-moist" cores (which are presumably more extreme in the case of the head fire plume) initiate the pyroCb, resulting in the observed rapid plume growth (Figure 1b) and plume top distribution (Figure 1a), which peaks at ~12.1 km. The photographs in Figures 4c

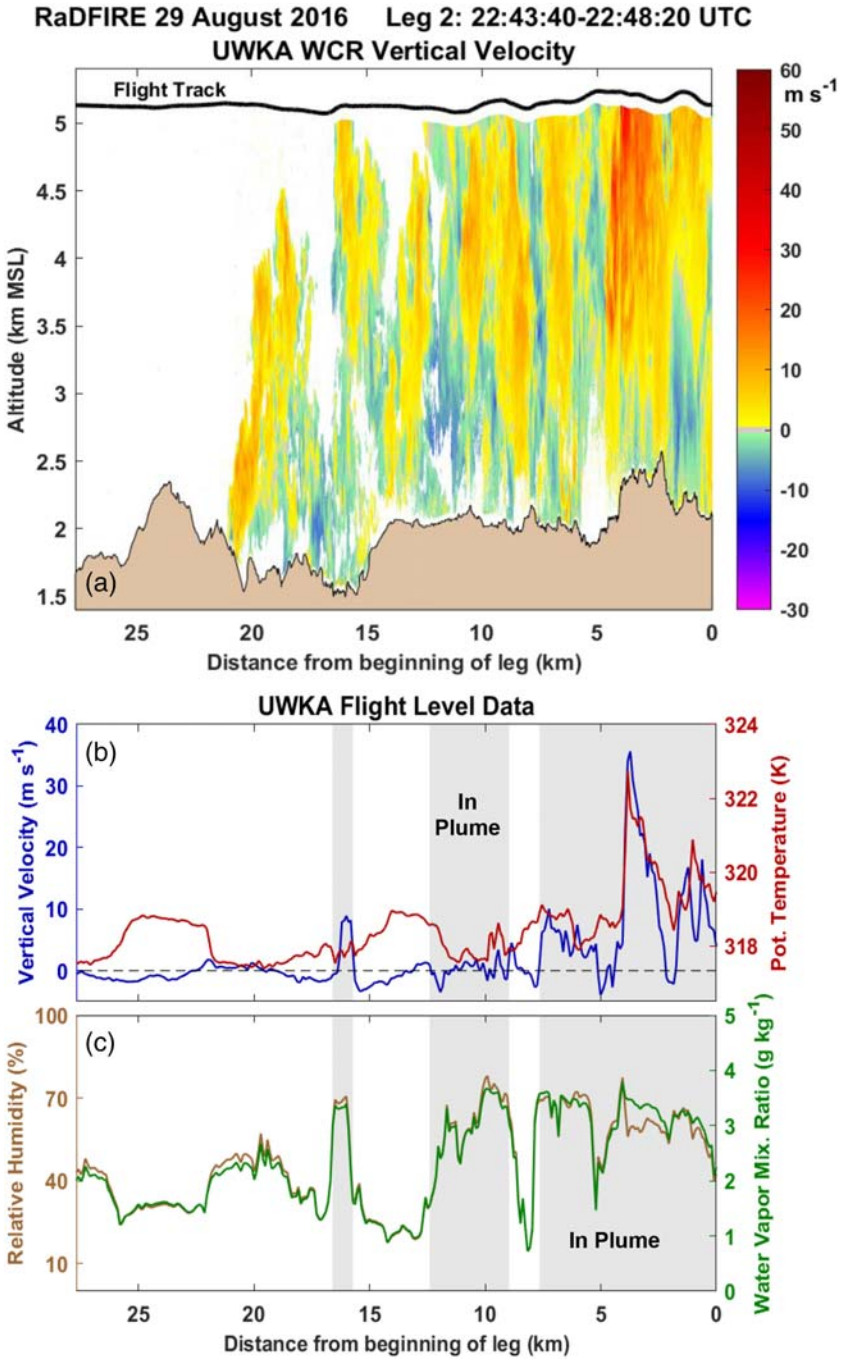

Figure 3. Overview of the aircraft penetration of the flanking plume. (a) Radar Doppler velocity (color shaded), terrain (beige), and flight altitude. (b) In situ potential temperature (red) and vertical velocity (blue). (c) In situ relative humidity (brown) and water vapor mixing ratio (green). In (b) and (c), the gray shading indicates times that the UWKA was "in-plume."

and 4d, along with that in Figure 1d, clearly show the transition from ash-filled to cloudy plume processes and the vigorous moist ascent aloft.

In light of these parcel estimates, it is notable that the observed updrafts (Figure 2d) peak below the estimated cloud base (~6 km) and that no secondary peak in vertical velocity occurs farther aloft, contrary to what would be expected due to moist-instability in pyroCb (Freitas et al., 2007; Trentmann et al., 2006). For example, the vertical velocity in the detached convective element above 6 km apparent in Figures 2a

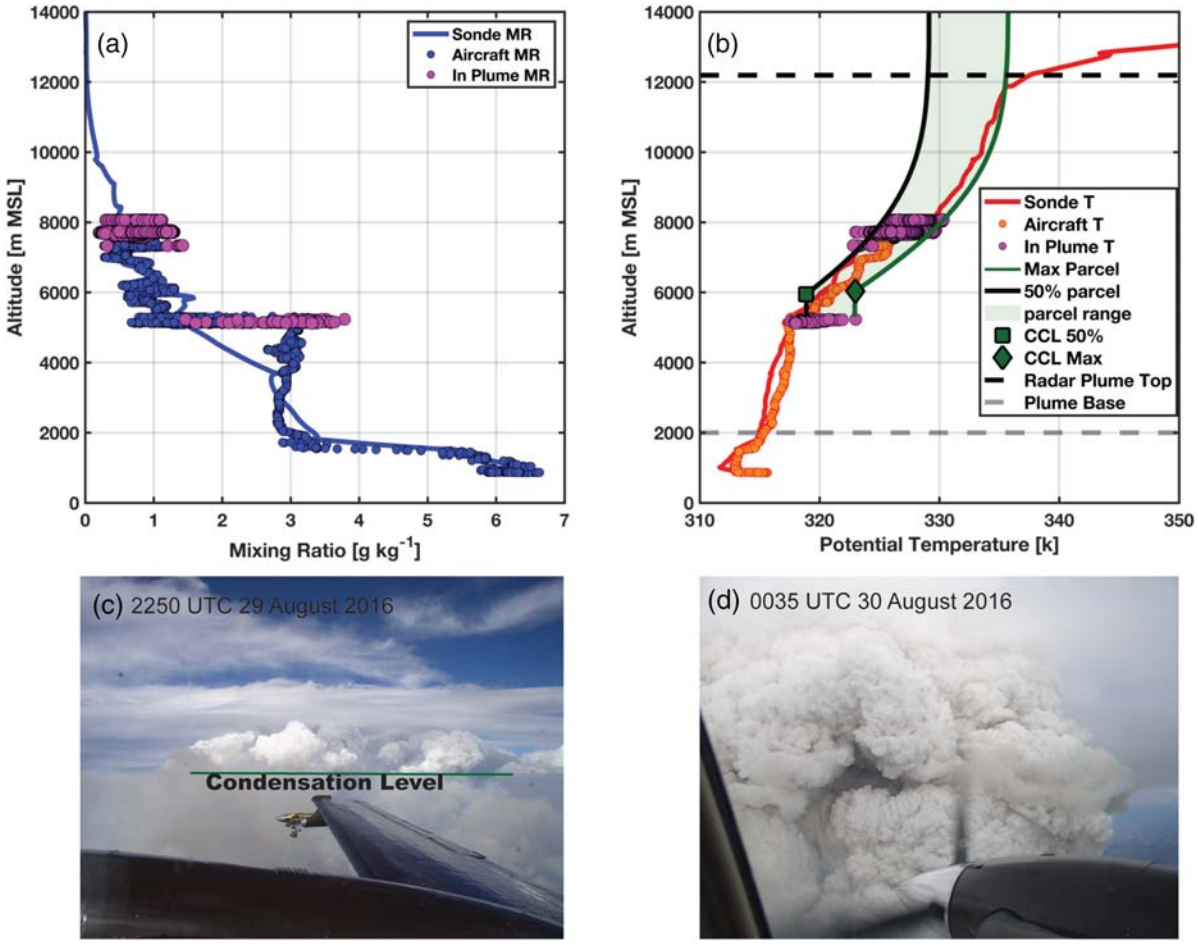

Figure 4. Overview of in-plume temperature and moisture observations relative to the ambient environment as measured by an aircraft ascent-descent sounding (dots) and the KBOI radiosonde (solid lines). (a) In-plume (magenta) and ambient (blue line, dots) water vapor mixing ratio observations. (b) In-plume (magenta) and ambient (red line, orange dots) potential temperature. Also shown in (b) are the parcel ascent estimates for the median (black) and maximum (green) in-plume values (see text). (c) Photo from the UWKA showing the transition from smoke-filled to cloudy plume (green line). (d) Photo from the UWKA showing vigorous convection in the cloudy portion of the plume. Note that the photograph times are shown in each panel, and the locations are presented in Figure 1a.

and 2b does not show an increase with height despite extending into the cloud. This is likely a result of a sampling bias due to the sloping plume geometry, evident in the KCBX data (Figure 1a) with the northeast displacement of the deep plume tops due to the ambient southwest wind. Safety precluded sampling in this region where further accelerations due to latent heat release may have yielded even stronger updrafts deep within the pyroCb. Future observations should attempt to resolve this portion of pyroCb-topped plumes.

4. Summary and Discussion

The vertical velocity and thermodynamic observations collected during the Pioneer Fire help address the question, "how strong are wildfire updrafts?" In short, they can be extreme, reaching at least 58 m s^{-1}, more than double previous estimates (Banta et al., 1992) and rivaling those in tornadic supercell thunderstorms, for which updraft speeds of 20–55 m s^{-1} have been observed and simulated (e.g., Miller et al., 1988; Trapp et al., 2017). While similar updraft magnitudes have been estimated immediately above flames during crown fires (Coen et al., 2004), the updrafts presented here occur far above the surface, are linked to wide updraft cores (e.g., 2 km), and, as we showed, play a key role in triggering the overlying pyroCb. As we have argued, the occurrence of these strong updrafts aloft is due to parcels remaining positively buoyant through a deep layer yielding sustained acceleration. While these plume cores remain positively buoyant, they have nevertheless incurred significant dilution with height due to entrainment of ambient air.

The magnitude and width of the observed updrafts have important implications for fire behavior. First, mass continuity requires strong inflow winds to replace the evacuated updraft air. These inflows are poorly understood yet can have a profound impact on the rate and direction of fire spread. Second, updrafts of this magnitude can loft large burning debris capable of initiating "spot fires" that merge to form "mass fire," which can feedback on fire intensity (Finney & McAllister, 2011). Third, these updrafts may help stretch, tilt, and twist fire-generated and ambient sources of vorticity, providing a pathway to tornado-strength vortices in wildfire plumes (Forthofer & Goodrick, 2011), including vortices linked to pyroCbs (e.g., Cunningham & Reeder, 2009; Lareau et al., 2018). Future investigations probing these feedbacks between updraft and fire are needed, especially in light of the increasing frequency, size, and impact of large wildfires (e.g., Dennison et al., 2014). Furthermore, it would be beneficial to leverage the dual-polarization capability of the WCR and NEXRAD in future research to improve our understanding of the structure and distribution of pyrometeors and hydrometeors in cases of deep pyroconvection.

We conclude by noting that extreme pyroconvective updrafts are also a previously undocumented aviation risk. Upon penetrating the 35 m s^{-1} updraft in the flanking plume (Figures 3a and 3b), the UWKA experienced a dramatic vertical displacement, injuring a flight scientist. Similarly, a Qantas Airlines flight en route to Canberra, Australia, was forced to make an emergency landing after encountering extreme turbulence in a developing pyroCu/Cb in January 2020 (Black & Hayne, 2020). Both the UWKA and Qantas pilots indicated their weather-avoidance radars did not alert them to these hazards, likely due to the low radar reflectivity of the pyrometeors (e.g., 25 dbZ in the updraft Figure 1c), as compared with the high reflectivity (50–75 dbZ) in precipitation-loaded thunderstorm updrafts, which are a well-known aviation hazard (Allen, 2013). Both pilots also reported dramatic reductions in ambient light within the plumes (i.e., nearly black), consistent with previous research flights documenting radiances reduced by several orders of magnitude in pyroCu plumes (Gatebe et al., 2012). Future guidelines concerning the dangers and radar reflectivity signatures of wildfire updrafts may be warranted.

Data Availability Statement

The UWKA data used in this study are available online (at http://flights.uwyo.edu/projects/radfire16/). The NEXRAD data are available online (at https://registry.opendata.aws/noaa-nexrad/). The radiosonde data are available at the UWYO website (http://weather.uwyo.edu/upperair/sounding.html).

Acknowledgments

Funding for this work is provided by the National Science Foundation under Grants AGS-1151930 and AGS-1719243. We acknowledge and thank efforts of staff at the University of Wyoming King Air Research Aircraft Facility in planning for, executing, and processing data collected from the aircraft mission described in this study.

References

Allen, J. (2013). Advisory circular 00–24°C. U.S. Department of Transportation Federal Aviation Administration. https://www.faa.gov/documentlibrary/media/advisory_circular/ac%2000-24c.pdf

Banta, R. M., Olivier, L. D., Holloway, E. T., Kropfli, R. A., Bartram, B. W., Cupp, R. E., & Post, M. J. (1992). Smoke-column observations from two forest fires using Doppler lidar and Doppler radar. *Journal of Applied Meteorology*, *31*(11), 1328–1349. https://doi.org/10.1175/1520-0450(1992)031<1328:SCOFTF>2.0.CO;2

Bargen, D. W., & Brown, R. C. (1980). Interactive radar velocity unfolding. *Preprints, 19th Conf. on Radar Meteor.*, Miami Beach, FL, Amer. Meteor. Soc., 278–283.

Black, M., & Hayne, J. (2020). Passengers describe flying through fire-generated cloud on Melbourne-to-Canberra flight. Australian Broadcasting Corporation. [accessed 2020 Feb 5]; 5 Jan 20. https://www.abc.net.au/news/2020-01-05/nsw-vic-fire-generated-thunderstorm-plane-qantas/11842038

Buckland, M. K. (2019). What is a megafire? Defining the social and physical dimensions of extreme US wildfires (1988-2014). Doctoral Dissertation, *University of Colorado at Boulder*.

Coen, J., Mahalingam, S., & Daily, J. (2004). Infrared imagery of crown-fire dynamics during FROSTFIRE. *Journal of Applied Meteorology*, *43*(9), 1241–1259. https://doi.org/10.1175/1520-0450(2004)043<1241:IIOCDD>2.0.CO;2

Cunningham, P., Goodrick, S. L., Hussaini, M. Y., & Linn, R. R. (2005). Coherent vortical structures in numerical simulations of buoyant plumes from wildland fires. *International Journal of Wildland Fire*, *14*(1), 61–75. https://doi.org/10.1071/WF04044

Cunningham, P., & Reeder, M. J. (2009). Severe convective storms initiated by intense wildfires: Numerical simulations of pyro-convection and pyro-tornadogenesis. *Geophysical Research Letters*, *36*, L12812. https://doi.org/10.1029/2009GL039262

Damiani, R., & Haimov, S. (2006). A high-resolution dual-Doppler technique for fixed multiantenna airborne radar. *IEEE Transactions on Geoscience and Remote Sensing*, *44*(12), 3475–3489. https://doi.org/10.1109/TGRS.2006.881745

Dennison, P. E., Brewer, S. C., Arnold, J. D., & Moritz, M. A. (2014). Large wildfire trends in the western United States, 1984–2011. *Geophysical Research Letters*, *41*, 2928–2933. https://doi.org/10.1002/2014GL059576

Eilts, M. D., & Smith, S. D. (1990). Efficient dealiasing of Doppler velocities using local environment constraints. *Journal of Atmospheric and Oceanic Technology*, *7*(1), 118–128. https://doi.org/10.1175/1520-0426(1990)007<0118:EDODVU>2.0.CO;2

Finney, M. A., & McAllister, S. S. (2011). A review of fire interactions and mass fires. *Journal of Combustion*, *2011*, 1–14. https://doi.org/10.1155/2011/548328

Forthofer, J. M., & Goodrick, S. L. (2011). Review of vortices in wildland fire. *Journal of Combustion*, *2011*, 1–14. https://doi.org/10.1155/2011/984363

Freitas, S. R., Longo, K. M., Chatfield, R., Latham, D., Silva Dias, M. A., Andreae, M. O., et al. (2007). Including the sub-grid scale plume rise of vegetation fires in low resolution atmospheric transport models. *Atmospheric Chemistry and Physics*, *7*(13), 3385–3398. https://doi.org/10.5194/acp-7-3385-2007

Fromm, M., Lindsey, D. T., Servranckx, R., Yue, G., Trickl, T., Sica, R., et al. (2010). The untold story of pyrocumulonimbus. *Bulletin of the American Meteorological Society*, *91*(9), 1193–1210. https://doi.org/10.1175/2010BAMS3004.1

Fromm, M., Tupper, A., Rosenfeld, D., Servranckx, R., & McRae, R. (2006). Violent pyro-convective storm devastates Australia's capital and pollutes the stratosphere. *Geophysical Research Letters*, *33*, L05815. https://doi.org/10.1029/2005GL025161

Gatebe, C. K., Varnai, T., Poudyal, R., Ichoku, C., & King, M. D. (2012). Taking the pulse of pyrocumulus clouds. *Atmospheric Environment*, *52*, 121–130. https://doi.org/10.1016/j.atmosenv.2012.01.045

Haines, D. A., & Smith, M. C. (1987). Three types of horizontal vortices observed in wildland mass and crown fires. *Journal of Climate and Applied Meteorology*, *26*(12), 1624–1637. https://doi.org/10.1175/1520-0450(1987)026<1624:TTOHVO>2.0.CO;2

Horel, J., Splitt, M., Dunn, L., Pechmann, J., White, B., Ciliberti, C., et al. (2002). Mesowest: Cooperative mesonets in the western United States. *Bulletin of the American Meteorological Society*, *83*(2), 211–225. https://doi.org/10.1175/1520-0477(2002)083<0211:MCMITW>2.3.CO;2

Lareau, N. P., & Clements, C. B. (2016). Environmental controls on pyrocumulus and pyrocumulonimbus initiation and development. *Atmospheric Chemistry and Physics*, *16*(6), 4005–4022. https://doi.org/10.5194/acp-16-4005-2016

Lareau, N. P., Nauslar, N. J., & Abatzoglou, J. T. (2018). The Carr Fire vortex: A case of pyrotornadogenesis? *Geophysical Research Letters*, *45*, 13–107.

Lindley, T. T., Speheger, D. A., Day, M. A., Murdoch, G. P., Smith, B. R., Nauslar, N. J., & Daily, D. C. (2019). Megafires on the southern Great Plains. *Journal of Operational Meteorology*, *7*(12), 164–179.

Luderer, G., Trentmann, J., & Andreae, M. O. (2009). A new look at the role of fire-released moisture on the dynamics of atmospheric pyro-convection. *International Journal of Wildland Fire*, *18*(5), 554–562. https://doi.org/10.1071/WF07035

McCarthy, N., Guyot, A., Dowdy, A., & McGowan, H. (2019). Wildfire and weather radar: A review. *Journal of Geophysical Research: Atmospheres*, *124*, 266–286. https://doi.org/10.1029/2018JD029285

Miller, L. J., Tuttle, J. D., & Knight, C. A. (1988). Airflow and hail growth in a severe northern High Plains supercell. *Journal of the Atmospheric Sciences*, *45*(4), 736–762. https://doi.org/10.1175/1520-0469(1988)045<0736:AAHGIA>2.0.CO;2

Peace, M., Mccaw, L., Santos, B., Kepert, J. D., Burrows, N., & Fawcett, R. J. (2017). Meteorological drivers of extreme fire behaviour during the Waroona bushfire, Western Australia, January 2016. *Journal of Southern Hemisphere Earth Systems Science*, *67*(2), 79–106. https://doi.org/10.22499/3.6702.002

Peterson, D. A., Hyer, E. J., Campbell, J. R., Solbrig, J. E., & Fromm, M. D. (2017). A conceptual model for development of intense pyro-cumulonimbus in western North America. *Monthly Weather Review*, *145*(6), 2235–2255. https://doi.org/10.1175/MWR-D-16-0232.1

Potter, B. E. (2005). The role of released moisture in the atmospheric dynamics associated with wildland fires. *International Journal of Wildland Fire*, *14*(1), 77–84. https://doi.org/10.1071/WF04045

Ray, P. S., & Ziegler, C. (1977). De-aliasing first-moment Doppler estimates. *Journal of Applied Meteorology*, *16*(5), 563–564. https://doi.org/10.1175/1520-0450(1977)016<0563:DAFMDE>2.0.CO;2

Thurston, W., Kepert, J. D., Tory, K. J., & Fawcett, R. J. (2017). The contribution of turbulent plume dynamics to long-range spotting. *International Journal of Wildland Fire*, *26*(4), 317–330. https://doi.org/10.1071/WF16142

Tory, K. J., Thurston, W., & Kepert, J. D. (2018). Thermodynamics of pyrocumulus: A conceptual study. *Monthly Weather Review*, *146*(8), 2579–2598. https://doi.org/10.1175/MWR-D-17-0377.1

Trapp, R. J., Marion, G. R., & Nesbitt, S. W. (2017). The regulation of tornado intensity by updraft width. *Journal of the Atmospheric Sciences*, *74*(12), 4199–4211. https://doi.org/10.1175/JAS-D-16-0331.1

Trentmann, J., Luderer, G., Winterrath, T., Fromm, M. D., Servranckx, R., Textor, C., et al. (2006). Modeling of biomass smoke injection into the lower stratosphere by a large forest fire (Part I): Reference simulation. *Atmospheric Chemistry and Physics*, *6*(12), 5247–5260. https://doi.org/10.5194/acp-6-5247-2006

Turner, J. S. (1962). The 'starting plume' in neutral surroundings. *Journal of Fluid Mechanics*, *13*(3), 356–368. https://doi.org/10.1017/S0022112062000762

Wang, Z., French, J., Vali, G., Wechsler, P., Haimov, S., Rodi, A., et al. (2012). Single aircraft integration of remote sensing and in situ sampling for the study of cloud microphysics and dynamics. *Bulletin of the American Meteorological Society*, *93*(5), 653–668. https://doi.org/10.1175/BAMS-D-11-00044.1

Werth, P. A., Potter, B. E., Clements, C. B., Finney, M. A., Forthofer, J. A., McAllister, S. S., & Cruz, M. G. (2011). Synthesis of knowledge of extreme fire behavior: Volume I for fire managers.

References From the Supporting Information

Haimov, S., & Rodi, A. (2013). Fixed-antenna pointing-angle calibration of airborne Doppler cloud radar. *Journal of Atmospheric and Oceanic Technology*, *30*(10), 2320–2335. https://doi.org/10.1175/JTECH-D-12-00262.1

Minder, J. R., Smith, R. B., & Nugent, A. D. (2013). The dynamics of ascent-forced orographic convection in the tropics: Results from Dominica. *Journal of the Atmospheric Sciences*, *70*(12), 4067–4088. https://doi.org/10.1175/JAS-D-13-016.1